HAL open science

Thermoelectric Scanning-Gate Interferometry on a Quantum Point Contact

B. Brun, F. Martins, S. Faniel, A. Cavanna, C. Ulysse, A. Ouerghi, U. Gennser, D. Mailly, P. Simon, S. Huant, et al.

▶ **To cite this version:**

B. Brun, F. Martins, S. Faniel, A. Cavanna, C. Ulysse, et al.. Thermoelectric Scanning-Gate Interferometry on a Quantum Point Contact. Physical Review Applied, 2019, 11 (3), pp.034069. 10.1103/PhysRevApplied.11.034069 . hal-02083926

HAL Id: hal-02083926

https://hal.science/hal-02083926v1

Submitted on 11 Aug 2023

HAL is a multi-disciplinary open access archive for the deposit and dissemination of scientific research documents, whether they are published or not. The documents may come from teaching and research institutions in France or abroad, or from public or private research centers.

L'archive ouverte pluridisciplinaire **HAL**, est destinée au dépôt et à la diffusion de documents scientifiques de niveau recherche, publiés ou non, émanant des établissements d'enseignement et de recherche français ou étrangers, des laboratoires publics ou privés.

Thermoelectric Scanning-Gate Interferometry on a Quantum Point Contact

B. Brun,[1,*] F. Martins,[1] S. Faniel,[1] A. Cavanna,[4] C. Ulysse,[4] A. Ouerghi,[4] U. Gennser,[4] D. Mailly,[4] P. Simon,[5] S. Huant,[2] M. Sanquer,[3] H. Sellier,[2] V. Bayot,[1] and B. Hackens[1]

[1] *NAPS/IMCN, Université Catholique de Louvain (UCLouvain), Chemin du Cyclotron 2, 1348 Louvain-La-Neuve, Belgium*

[2] *QNES, Institut Néel, Université Grenoble Alpes, CNRS, 25 Avenue des martyrs, 38000 Grenoble, France*

[3] *Pheliqs/INAC, Université Grenoble Alpes, CEA, 17 Avenue des Martyrs, 38000 Grenoble, France*

[4] *C2N, CNRS, 10 Boulevard Thomas Gobert, 91120 Palaiseau, France*

[5] *LPS/CNRS, Université Paris Sud, 1 rue Nicolas Appert, 91405 Orsay, France*

(Received 30 March 2018; revised manuscript received 30 January 2019; published 28 March 2019)

We introduce a scanning probe technique derived from scanning gate microscopy (SGM) to investigate thermoelectric transport in two-dimensional semiconductor devices. Thermoelectric scanning gate microscopy (TSGM) consists in measuring the thermoelectric voltage induced by a temperature difference across a device while scanning a polarized tip that locally changes the potential landscape. We apply this technique to perform interferometry of the thermoelectric transport in a quantum point contact (QPC). We observe an interference pattern in both SGM and TSGM images, and evidence large differences between the two signals in the low-density regime of the QPC. In particular, a large phase jump appears in the interference fringes recorded by TSGM, which is not visible in the interference fringes recorded by SGM. We discuss this difference of sensitivity using a microscopic model of the experiment, based on the contribution from a resonant level inside or close to the QPC. This work demonstrates that combining scanning gate microscopy with thermoelectric measurements offers new information as compared with SGM alone, and provides direct access to the derivative of the device transmission with respect to energy, both in amplitude and in phase.

DOI: 10.1103/PhysRevApplied.11.034069

I. INTRODUCTION

In the context of emerging quantum technology and in view of the increasing concern for energy harvesting, thermoelectric transport in nanomaterials and nanodevices has recently regained interest [1,2]. This has led to alternative quantum thermal devices such as caloritronic interferometers [3]. The ability to accurately measure heat transport in two-dimensional systems [4] and atomic junctions [5] improved our global understanding of quantum thermodynamics, and shed light on the mechanisms at play in complex many-body problems [6–8]. Investigating these thermal effects at the local scale is challenging, but much effort is being made in this direction. As an example, heat dissipation was recently mapped inside a graphene nanodevice with unprecedented thermal resolution and spatial resolution [9], unveiling new mechanisms responsible for current-to-heat conversion in graphene [10].

Here we introduce a scanning probe technique based on the Seebeck effect to investigate the temperature-to-voltage conversion at the local scale within a quantum device [11,12]. This technique, which we call "thermoelectric scanning gate microscopy" (TSGM), is applied to study the puzzling low-density regime of quantum point contacts (QPCs) [13,14]. Our experiments unveil unexpected features in the thermopower that are not visible in conductance measurements. We explain these deviations by the enhanced sensitivity of the thermopower to phenomena occurring at low transmission. This observation may help to clarify the nature of the conductance and thermoelectric anomalies in QPCs.

QPCs are quasi-one-dimensional ballistic channels in high-mobility two-dimensional electron gases (2DEGs). Their curves of conductance versus split-gate voltage show quantized plateaus at integer multiples of $2e^2/h$ as a consequence of ballistic transport [15]. They also show anomalous features that are believed to result from electron-electron (e-e) interactions. The conductance exhibits a shoulderlike feature known as the 0.7 anomaly [16], which disappears as the temperature is lowered. Additionally, the differential conductance exhibits a zero-bias peak at very low temperature, known as the zero-bias anomaly [17]. Many different models have been proposed to explain these anomalies, but after decades of investigations, their exact microscopic origin still remains a matter of intense debate [16–25].

*boris.brun@uclouvain.be

 © 2019 American Physical Society

The thermoelectric properties of QPCs have also been studied [26] and were shown to be excellent probes of quantum confinement effects. The Seebeck coefficient $S = (\partial V/\partial T)_{I=0}$ relates variations of voltage V to temperature T in the absence of current I. It has been shown to oscillate with the number of transmitted modes in the QPC [27]. The thermal conductance and Peltier coefficients show similar behavior [28].

In a single-electron picture, S is linked to the conductance G through Mott's relation [29]:

$$S^M(\mu, T) = -\frac{\pi^2 k_B^2 T}{3e}\frac{1}{G(\mu, T)}\frac{\partial G(\mu, T)}{\partial \mu}, \qquad (1)$$

where μ is the chemical potential. However, the thermopower is predicted to be sensitive to *e*-*e* interactions, and often reveals different information compared with the conductance. For example, in the case of Coulomb blockade, thermopower measurements probe the excitation spectrum rather than the addition spectrum [30,31]. Since the thermopower is sensitive to the slope of the local density of states, it may be a useful probe of correlated behavior [32,33], which makes it very relevant in the case of QPC anomalies. Large deviations from Eq. (1) have been reported in QPCs below the first conductance plateau [34], and were attributed to the important role of *e*-*e* interactions in this regime.

In this paper, we present an additional perspective on the low-transmission regime of QPCs through interferometric Seebeck measurements performed with our TSGM technique. This microscopy mode is a variant of scanning gate microscopy (SGM), where the negatively polarized tip of a low-temperature scanning probe microscope is scanned above the surface while recording tip-induced changes in the device's conductance [35,36]. In TSGM, the device's Seebeck coefficient S is recorded instead of its electrical conductance [37]. One of the two electron reservoirs is heated with a low frequency alternating current and the thermovoltage V_{th} across the device is measured as a function of the tip position [Fig. 1(a)]. The Seebeck coefficient is obtained as $S = V_{\text{th}}/\Delta T$, where ΔT is the temperature difference [Fig. 1(b)].

In SGM images of QPCs, when the tip voltage is chosen such as to locally deplete the 2DEG, it generates fringes spaced by half of the Fermi wavelength due to Fabry-Perot interference between the depleted region below the tip and the constriction defined by the split gate [35,38,39]. These fringes are observed in both SGM and TSGM images, but with significant differences near the QPC pinch-off. These differences cannot be explained in the framework of Mott's relation [Eq. (1)], indicating the crucial role played by the electron interactions in this regime. Understanding this many-body physics has been a research topic for decades, and is beyond the scope of the present paper.

Instead, we analyze in more detail the thermoelectric-scanning-gate-interferometry technique in a single-particle framework. We propose a microscopic model incorporating the contribution of a resonant energy level located close to the QPC to simulate the SGM and TSGM signals. We show explicitly that the different connection of G and S to the slope of the density of states at the Fermi energy results in enhanced sensitivity of S to localized states with weak transmission. This property makes the TSGM technique particularly relevant for the investigation of the low-density regime of QPCs, where spontaneous localized states have been predicted [40] and observed [17,41].

II. DESCRIPTION OF THERMOPOWER MEASUREMENTS

The device chosen to illustrate this new experimental technique is a QPC, defined in a GaAs/(Al,Ga)As heterostructure by a 270-nm-long and 300-nm-wide gap of a Ti/Au split gate. The 2DEG located 105 nm below the surface has electron density of 2.5×10^{15} m^{-2} and electronic mobility 1.0×10^6 cm^2/V s at 4 K. The device is thermally anchored to the mixing chamber of a dilution fridge in front of a cryogenic scanning probe microscope [42] and cooled to a base temperature of 25 mK. The four-probe differential conductance is measured by a lock-in technique with 10-μV excitation at 77 Hz. A series resistance of 200 Ω is subtracted from all the data to have the first conductance plateau at $2e^2/h$. The lever-arm parameter of the split gate $\alpha = 54$ meV/V is deduced from nonlinear spectroscopy of the QPC subbands separated by $\Delta E = 3.5$ meV (see Fig. S1 in Supplemental Material [43]).

To measure the Seebeck coefficient of the QPC, we use the electron-heating technique depicted in Fig. 1(a). We inject an alternating current at 7.17 Hz between two contacts on the same side of the QPC and record the voltage across the QPC using lock-in detection at twice the heating frequency (14.34 Hz) to be sensitive to the dissipated power only and avoid any contribution related to the electrical conductance [28]. The thermovoltage recorded versus gate voltage V_g is shown in Fig. 1(c) together with the measured conductance curve. As expected theoretically [26], the thermovoltage oscillates between minimum values when the QPC is on a plateau and maximum values for transitions between plateaus. For comparison, the transmission and Seebeck coefficients expected from a noninteracting-saddle-point model [15] are plotted in Fig. 1(d).

A crucial issue in thermopower measurements is to relate the applied heating current to an actual temperature difference ΔT. To evaluate this quantity, we use two independent methods. First, we use Mott's law for high densities, assuming that it is valid when more than two

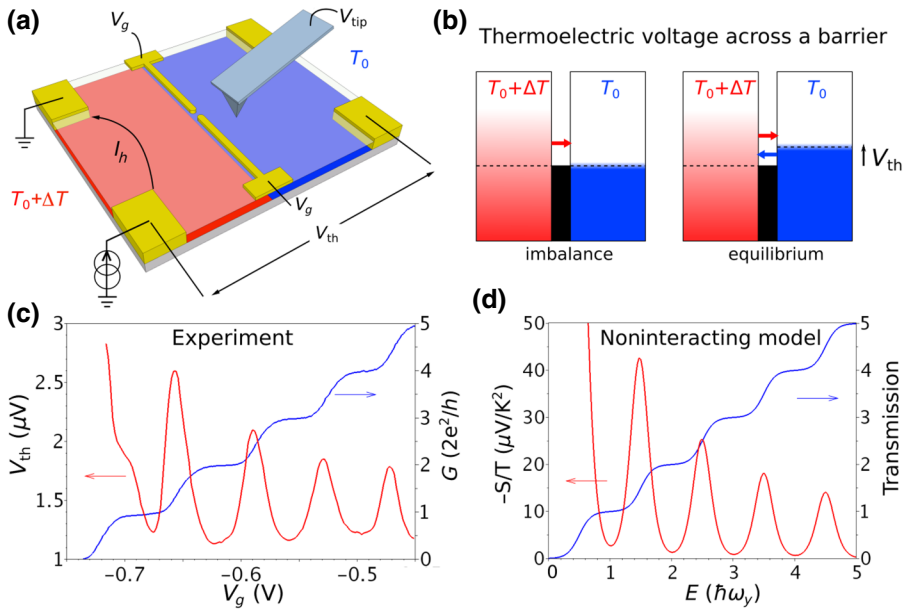

FIG. 1. (a) The TSGM experiment: one side of the device is brought to higher temperature and the thermovoltage is recorded while scanning the polarized tip. (b) Seebeck effect across a barrier (black region): red and blue bars illustrate the energy distribution of charge carriers on the hot and cold sides. If transmission is energy dependent, fluxes of hot and cold carriers are imbalanced. At equilibrium, a charge accumulation on the cold side restores the total balance of fluxes: this increases the thermovoltage $V_{\rm th}$. (c) Differential conductance G measured with a four-probe technique at 25 mK (blue) and thermovoltage measured with a heating current of 180 nA (red) versus gate voltage V_g. (d) Theoretical transmission (blue) and Seebeck coefficient (red) calculated from the saddle-point model [15] versus energy for $\omega_x/\omega_y = 0.6$.

modes are transmitted through the QPC, and compare quantitatively the measured value S with that predicted by Mott's law S^M. This comparison indicates the existence of a heating-current-dependent but gate-voltage-independent background in the measured signal (see Fig. S3 in Supplemental Material [43]). With this background contribution removed, the measured Seebeck coefficient should be given by Mott's relation applied to the measured conductance [black curve in Fig. 2(a)]. This is well verified for the third to fifth transitions, the only fitting parameter being the temperature difference.

Figure 2(b) shows the temperature differences deduced from these assumptions, ranging from 100 to 800 mK for heating currents from 15 to 400 nA. Second, we compare these extracted values with estimates obtained from the temperature and current dependence of the Shubnikov–de Haas oscillations in our sample, and find good agreement (see Fig. S4 in Supplemental Material [43]). The temperature difference is always larger than the average temperature, such that the system is far from the linear regime. Nevertheless, it has been shown that Mott's law holds even in this highly nonlinear regime provided that ΔT is smaller than the subband spacing and smearing [44].

The electronic temperature in the middle of the heated reservoir evolves sublinearly with the heating current I_h, whereas one could naively expect a I_h^2 dependence related to the dissipated Joule power. This can be explained by the nonlinear temperature dependence of heat losses in 2DEGs, mostly due to phonon emission [45] and electron out-diffusion in the Ohmic contacts [4,7]. These competing losses yield a nonuniform temperature profile and a sublinear dependence on I_h of the local temperature far from the Ohmic contacts [46–49].

In Fig. 2(a), the correspondence between S and S^M does not hold when fewer than three QPC modes are transmitted, with three distinct features highlighted by the plot of their difference [see Fig. 2(c)]: (i) in the transition from pinch-off to the first plateau ($V_g \sim -0.74$ to -0.71 V), the difference is very large (positive) and increases with decreasing temperature; (ii) on the first plateau ($V_g \sim -0.71$ to -0.68 V), the difference is of opposite sign (negative) and forms a peak at the lowest temperatures; (iii) in the transition from the first to the second plateau ($V_g \sim -0.68$ to -0.64 V), a large difference (positive) arises as ΔT is lowered below 500 mK.

Differences between S and S^M in the low-density regime of QPCs were reported in Ref. [34]. In that work, a local minimum was observed in the thermopower at the position of the $0.7 \times 2e^2/h$ anomalous conductance plateau at 2 K, as expected from Eq. (1). However this minimum was shown to disappear into a shoulder at the lowest temperature of 300 mK, whereas the 0.7 plateau was still present [deviation from Eq. (1)].

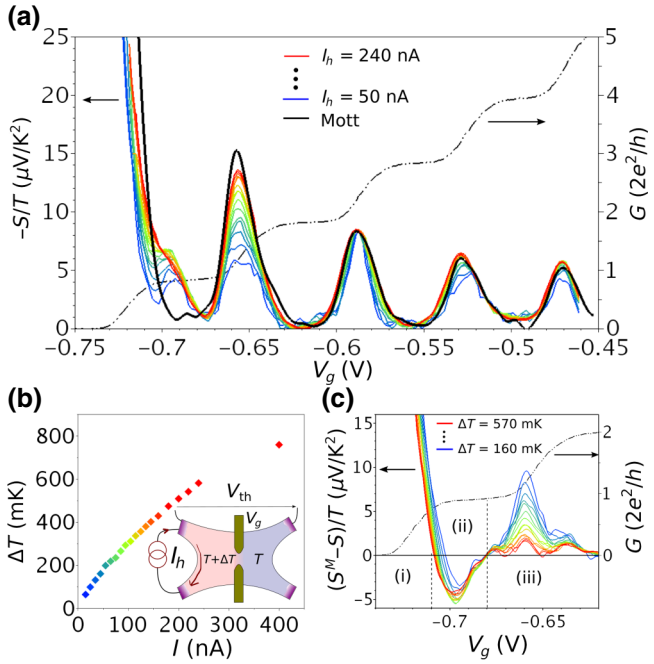

FIG. 2. (a) The black curve represents $-S^M/T$ calculated with Mott's law from the $G(V_g)$ curve at 25 mK (dashed line). The colored curves represent $-S/T = (V_{\rm th}/\Delta T)/T_{\rm average}$ scaled to the black curve at the third peak summit with ΔT as the only fitting parameter. The heating currents range from 50 to 240 nA (blue to red). (b) Temperature difference ΔT as a function of the heating current. The inset shows an electron-microscope image of the device. The scale bar is 5 μm. (c) $S/T - S^M/T$ for temperature differences from 160 to 570 mK (blue to red) as a function of V_g. Same data as in (a).

Here the thermopower is also in contradiction with Mott's law but in a different way. The base temperature is much lower (25 mK) and the conductance curve does not show any 0.7 plateau (an absence related to the emergence of a zero-bias peak in the differential conductance [17]). The thermopower, however, shows a peak at the lowest temperatures and a minimum around $V_g = -0.705$ V that disappears for ΔT greater than 500 mK [Fig. 2(a)].

III. THERMOELECTRIC SCANNING GATE MICROSCOPY

We now report on the TSGM experiment (i.e., the investigation of thermoelectric transport in the presence of the scanning gate). The tip is scanned 50 nm above the sample surface with an applied voltage of -6 V, which locally depletes the 2DEG. Figure 3(a) and 3(b) shows the SGM and TSGM images obtained by our recording successively the conductance and the thermoelectric voltage in two different tip scans. The conductance signal is recorded with an ac excitation of 10 μV, and the thermovoltage is recorded with a heating current of 150 nA, corresponding to a temperature difference of 450 mK. Both images look very similar, presenting interference fringes due to the Fabry-Perot cavity formed by the QPC and the tip-depleted region. The TSGM image provides, to our knowledge, the first observation in real space of a thermally driven electron interferometer.

Despite their apparent similarities, these images carry distinct information and one cannot be deduced from the other. Indeed, even in the range where Mott's relation (1) is valid, deducing the TSGM image $S(x_{\rm tip}, y_{\rm tip})$ from the SGM image $G(x_{\rm tip}, y_{\rm tip})$ would require a knowledge of how the transmission evolves with the chemical potential ($\partial G/\partial\mu$). Mostly, this quantity is not available in a GaAs 2DEG since it requires a backgate to vary the global electron density[50,51], which is a real challenge in high-mobility GaAs heterostructures.

In Fig. 2(a), the chemical potential of the QPC itself is identified as being proportional to V_g, which is a reasonable approximation when considering only the QPC transmission. In TSGM images, the distant influence of the tip does not allow such an identification, since the system studied now consists of the QPC coherently coupled to the tip-induced Fabry-Perot cavity. As a consequence, the chemical potential of the system is not linearly linked to V_g, and TSGM images provide information different from that obtained by SGM.

To illustrate these differences, we study the evolution of the interference fringes as a function of the QPC opening. The conductance G and the thermovoltage $V_{\rm th}$ are recorded separately while the tip is scanned along the line shown in Figs. 3(a) and 3(b), with an excitation of 15 μV and a temperature difference of 450 mK for G and S measurements, respectively. The evolution of the interference fringes with V_g is shown in Figs. 3(c) and 3(d) for the conductance and thermovoltage signals. The fringes are similar in both signals but are superimposed on two very different background signals: a series of conductance plateaus for G and a series of peaks for $V_{\rm th}$ (see Fig. 2), including a very strong peak at the QPC pinch-off. To highlight the fringes' evolution with V_g, we plot the first derivative of both signals with respect to the tip position along the red line, $d_{\rm tip}$, in Figs. 3(e) and 3(f). In these maps, we observe a complex evolution of the interference fringes, which looks globally similar in G and S, although a few differences can be detected.

In the following, we focus on the low-conductance regime, below approximately $0.5 \times 2e^2/h$, where S and S^M differ by a large amount [Fig. 2(c)]. In this regime, the SGM and TSGM interferometric signals evolve differently with gate voltage. The conductance oscillations follow a monotonic behavior [Figs. 4(c) and 4(e)] (i.e., their phase evolves monotonically with gate voltage), whereas the thermopower oscillations exhibit an abrupt phase shift at a conductance of about $0.25 \times 2e^2/h$ [Figs. 4(d) and 4(f)], which can also be surmised from Figs. 3(d) and 3(f). A Fourier analysis [Fig. 4(e)] indicates that the phase shift

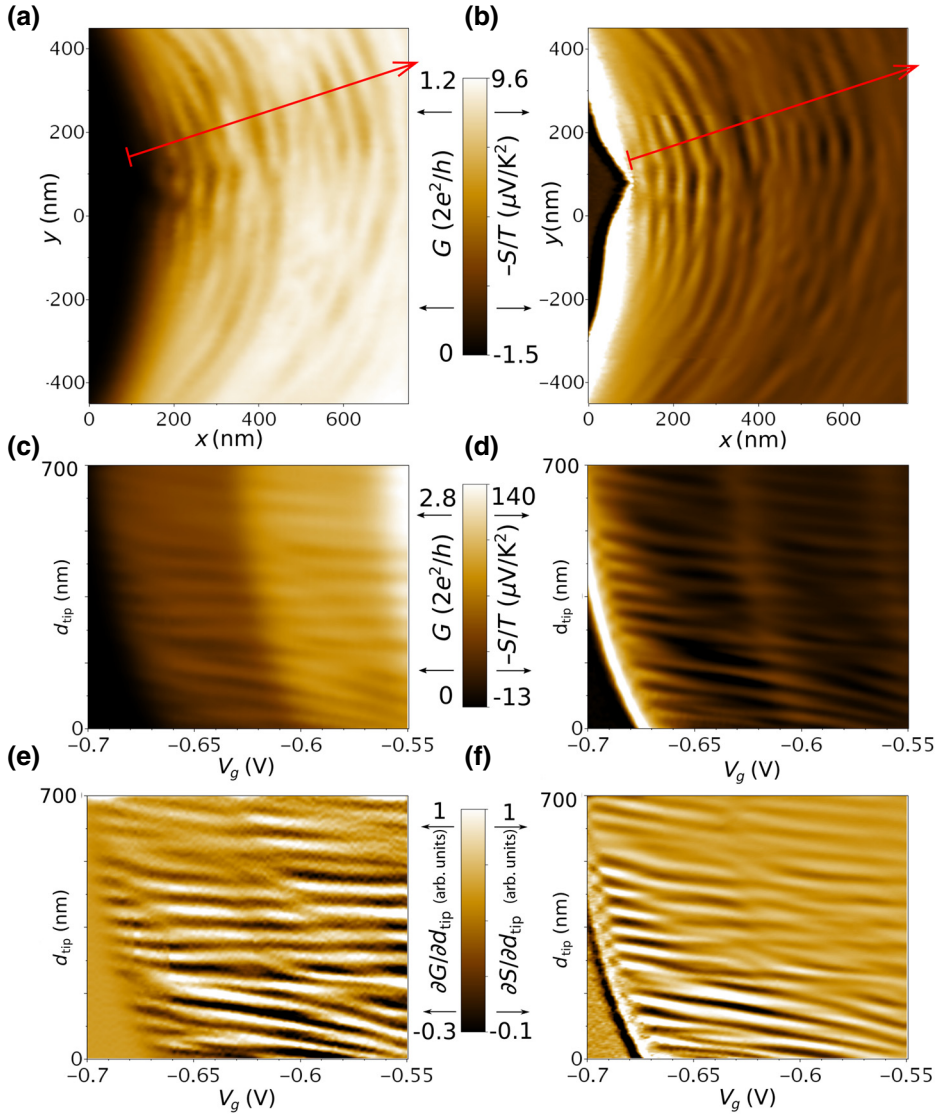

FIG. 3. (a) SGM image recorded when the QPC is open on the first plateau ($V_g = -0.66$ V): conductance G as a function of tip coordinates. The QPC center is located at $(-150; 0)$ nm on the left side of the image. (b) TSGM image of the thermopower in the same conditions, but recorded in a second pass while the reservoir is being heated on the opposite side of the scanning area. (c) Conductance and (d) thermovoltage as a function of gate voltage and tip position along the red line drawn in (a),(b) recorded in the same conditions but in separate tip scans. (e),(f) Derivative of (a),(b) with respect to tip position.

observed in the thermopower is almost π. Similar phase shifts were observed in the conductance signal in many different devices in our previous experiments [52]. However, they were observed at higher transmission, close to the first conductance plateau. Here the phase shift is observed in the thermopower at very low transmission, where no phase shift is present in the conductance.

IV. DISCUSSION

Phase shifts in the conductance were previously observed in Aharonov-Bohm interferometers containing a quantum dot in one arm, where the interference pattern experiences a phase shift by π whenever one charge is added to the quantum dot [53] and by $\pi/2$ in the Kondo regime [54].

Similarly, the phase shift observed in our SGM-based interferometry experiment indicates the presence of a resonant level in the cavity formed by the QPC and the tip. Such a resonant level could be located in the QPC itself, as reported in Ref. [22], or in the 2DEG region between the QPC and the tip, as a result of potential fluctuations induced by remote ionized dopants. In the latter case, the phase shift of the interference pattern would barely depend on the QPC gate voltage. Experimentally, however, the phase shift evolves with gate voltage following exactly

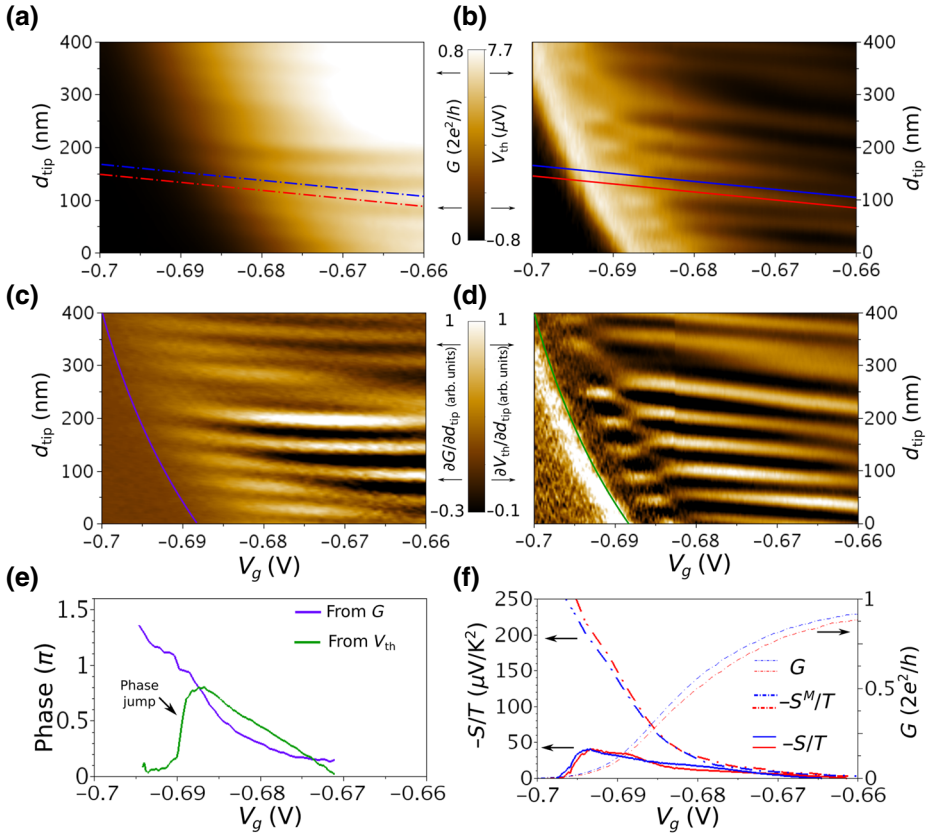

FIG. 4. (a) Conductance and (b) thermovoltage as a function of gate voltage and tip position along the red line drawn in Fig. 3, where d_{tip} here denotes tip position between 250 and 650 nm in Figs. 3(c)–3(f). (c),(d) Derivative of (a),(b) with respect to tip position. (e) Phase of the interference fringes as a function of gate voltage extracted from the conductance (purple) and thermovoltage (green) following the pinch-off lines shown in (c),(d) to account for a cross-talk effect. (f) Line profiles of G, $-S^M/T$, and $-S/T$ extracted along the red and blue lines in (a),(b).

the QPC pinch-off line [Fig. 4(d)], suggesting that this resonant state is in the vicinity of the QPC.

Although this localized state could result from disorder in the potential of the QPC channel, it could also correspond to a spontaneously localized charge. Indeed, several pieces of evidence for the existence of bound states in QPCs near pinch-off have been reported [41,55–59]. Such bound states have been predicted to spontaneously form in QPCs in several numerical studies [60–64] as a consequence of *e-e* interactions. When the potential barrier of the QPC is above the Fermi level, there are two regions of low density, one on each side of the barrier, where charges could spontaneously localize. Numerical simulations of this peculiar situation encountered near pinch-off support the presence of bound states [65,66] detected in coupled-QPC experiments [57,67]. This scenario was also proposed in Ref. [68] to explain the presence of QPC conductance anomalies down to very low conductance. This is also consistent, for example, with the results of local-spin-density-functional theory presented in Ref. [18], where two charges are shown to be localized on both sides of the main barrier at low density. Finally, classical electrostatic simulations also confirm that at low QPC transmission, two one-dimensional regions form on both sides of the channel, where the density is low enough to induce Wigner crystallization [69,70] (see Sec. VI in Supplemental Material [43]).

Some experiments [71], however, found no sign of such a localized state, and some theoretical studies proposed an alternative explanation for the related 0.7 and zero-bias anomalies [20,72], without invoking the presence of a localized charge. Also, in presence of interactions, Friedel oscillations between the QPC barrier and the SGM tip [60,73] could give rise to a phase shift of the interference pattern, but this effect is not expected to appear as abruptly versus gate voltage as is observed here.

In conclusion, the phase shift observed here by TSGM at very-low transmission is probably related to the presence of a localized state on the side of the QPC, but distinguishing whether this state is induced by *e-e* interaction or by disorder is beyond the scope of the present paper and would require additional investigation.

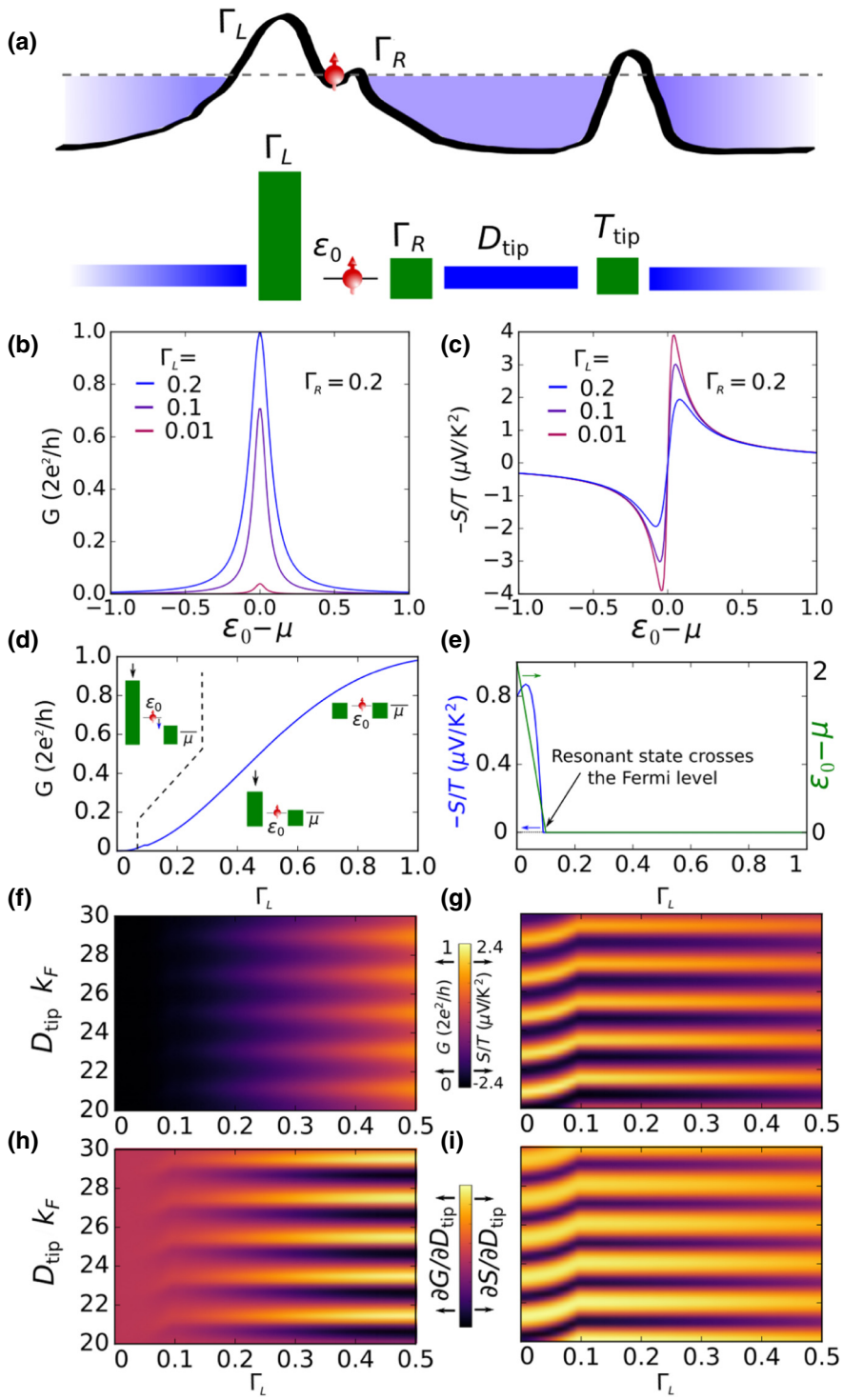

FIG. 5. (a) The top scheme shows a typical energetic potential that could lead to the proposed scenario: a localized state is located on the tip side of the main QPC barrier. The bottom scheme shows the one-dimensional model including, from left to right, the QPC barrier (Γ_L), the localized state (ϵ_0 and Γ_R), and the tip-induced cavity (D_{tip} and T_{tip}). (b) Conductance of the resonant level as a function of its energy relative to μ for fixed $\Gamma_R = 0.2$ and $\Gamma_L = 0.2$ (blue) to 0.01 (red). (c) Seebeck coefficient in the same configuration. (d) Conductance evolution with Γ_L assuming that the resonant level, perfectly coupled to the right lead ($\Gamma_R = 1$), crosses μ at $\Gamma_L = 0.1$ and then stays just below the Fermi level while the QPC opens. (e) Seebeck coefficient in the exact same scenario. (f),(g) Evolution of the Fabry-Perot interference in this scenario: conductance (f) and Seebeck coefficient (g) as a function of tip distance and Γ_L. (h),(i) Derivative of G and S with respect to D_{tip}.

V. EFFECT OF A LOCALIZED STATE IN TSGM INTERFEROMETRY

In this section, we use a simple microscopic model to analyze the effect of a localized state (irrespective of its origin in this specific sample) on the SGM and TSGM interferometric signals. We model the gate-controlled potential in the QPC by a barrier with transmission rate Γ_L and we assume the presence of a localized state on the right side of the barrier, at energy ϵ_0, separated from the right reservoir by a barrier with transmission rate Γ_R [Fig. 5(a)]. We model the tip as a distant scatterer of transmission amplitude $T_{\text{tip}} = 0.99$, whose distance from the resonant level D_{tip} can be varied. The expression for the energy-dependent transmission $T(E)$ through the whole system can then be calculated exactly as presented in Ref. [22]. In the Landauer framework, G and S are expressed as [74]

$$G = \frac{2e^2}{h} L_0, \tag{2}$$

$$S = -\frac{1}{|e|T}\frac{L_1}{L_0}, \tag{3}$$

where

$$L_m = \int_{-\infty}^{+\infty} (E-\mu)^m \left(\frac{\partial f}{\partial E}\right) T(E)\, dE, \tag{4}$$

where $f(E)$ is the Fermi distribution.

We first show that the behaviors with respect to the tunneling rates of asymmetric barriers are very different for G and S [Figs. 5(b) and 5(c)]. For a fixed tunneling rate $\Gamma_R = 0.2$ (in the unit of the hopping term t), the effect of a decrease in Γ_L is opposite for G and S: it tends to decrease G, which is dominated by the lowest tunneling rate, but to increase S on both sides of the resonance since it is sensitive to the resonance sharpness, and thus inversely proportional to $\Gamma_{\text{tot}} = \Gamma_L + \Gamma_R$.

In the following, we assume that the resonant state is very well coupled to the right lead (Γ_R fixed at 1) and that it evolves with Γ_L as shown in the inset in Fig. 5(e). As the QPC is progressively opened from the pinch-off (increase of Γ_L), the energy of the resonant state ϵ_0 drops until it reaches the Fermi level at $\Gamma_L = 0.1$ [dashed line in Fig. 5(d)]. Opening the QPC further does not change ϵ_0, but the level stays pinned close to μ, up to the point where $\Gamma_L = \Gamma_R$ and the transmission reaches unity. In this scenario, the conductance behaves as normally expected for a QPC [Fig. 5(d)]: the resonance is almost invisible as it appears close to the pinch-off. It also gives no discernible signature in the interference fringes, since it occurs at very low transmission [Figs. 5(f) and 5(h)]. The high sensitivity of S results from the strong variation of the transmission with energy when the resonance approaches the Fermi level.

The phase shift induced by the drop of ϵ_0 below μ is highly visible in S, and is due to the Breit-Wigner-like resonance of the localized state, which induces a total π phase shift when the level crosses the Fermi energy. Since the Fabry-Perot cavity probes twice the resonant-level phase shift in the case of strong coupling on the cavity side [22], the total phase shift should be 2π. However, assuming that the ϵ_0 level falls just below μ but remains at a constant energy value, the phase shift remains half the value of 2π, which corresponds to the experimentally observed value π. This model therefore provides a plausible scenario to understand our TSGM-interferometry results

VI. CONCLUSION

In conclusion, we introduce a new scanning probe technique to image thermoelectric transport through a QPC. By scanning the polarized tip in front of the QPC, we image the interference of electrons driven by a temperature difference, in analogy with the well-established SGM experiments where the electron flow is driven by a voltage difference. In addition, we show that in the very-low-conductance regime, the thermopower interference fringes experience an abrupt phase shift, invisible in the conductance signal. We propose a simple one-dimensional model to show that this phase shift and its characteristics can be explained by the contribution of a localized state inside or close to the QPC and that stays pinned to the Fermi energy of the leads as the first QPC mode opens. The fact that this localized-state signature is hidden in conductance measurements but is highly visible in the Seebeck coefficient is explained by its sharpness and occurrence at low transmission. This work illustrates that the combination of scanning gate microscopy and thermoelectric measurements can unveil elusive phenomena that escape transport measurements. Although we cannot draw definitive conclusions on the mechanism leading to this localization, we provide a tool that may prove useful in future investigations of conductance and thermoelectric anomalies in QPCs.

ACKNOWLEDGMENTS

We thank J.-L. Pichard and A. Abbout for the original idea for the experiment. This work was supported by Crédit de Recherche Grant No. J.0009.16 from the Fonds de la Recherche Scientifique-Fonds National de la Recherche Scientifique (FNRS), and the French Agence Nationale de la Recherche (ITEM-exp project). B.B, F.M., and B.H. acknowledge support from the Belgian Fonds Spéciaux de Recherche-FNRS, S.F. received support from the FSR at Université catholique de Louvain.

B.B. and F.M. contributed equally to this work.

[1] M. Dresselhaus, G. Chen, M. Tang, R. Yang, H. Lee, D. Wang, Z. Ren, J.-P. Fleurial, and P. Gogna, New directions for low-dimensional thermoelectric materials, Adv. Mater. **19**, 1043 (2007).

[2] J.-H. Jiang and Y. Imry, Linear and nonlinear mesoscopic thermoelectric transport with coupling with heat baths, C. R. Phys. **17**, 1047 (2016).

[3] F. Giazotto and M. J. Martínez-Pérez, The Josephson heat interferometer, Nature **492**, 401 (2012).

[4] S. Jezouin, F. D. Parmentier, A. Anthore, U. Gennser, A. Cavanna, Y. Jin, and F. Pierre, Quantum limit of heat flow across a single electronic channel, Science **342**, 601 (2013).

[5] L. Cui, W. Jeong, S. Hur, M. Matt, J. C. Klöckner, F. Pauly, P. Nielaba, J. C. Cuevas, E. Meyhofer, and P. Reddy, Quantized thermal transport in single-atom junctions, Science **355**, 1192 (2017).

[6] M. Banerjee, M. Heiblum, A. Rosenblatt, Y. Oreg, D. E. Feldman, A. Stern, and V. Umansky, Observed quantization of anyonic heat flow, Nature **545**, 75 (2017).

[7] E. Sivre, A. Anthore, F. D. Parmentier, A. Cavanna, U. Gennser, A. Ouerghi, Y. Jin, and F. Pierre, Heat Coulomb blockade of one ballistic channel, Nat. Phys. **14**, 145 (2017).

[8] B. Dutta, J. T. Peltonen, D. S. Antonenko, M. Meschke, M. A. Skvortsov, B. Kubala, J. König, C. B. Winkelmann, H. Courtois, and J. P. Pekola, Thermal Conductance of a Single-Electron Transistor, Phys. Rev. Lett. **119**, 077701 (2017).

[9] D. Halbertal, J. Cuppens, M. B. Shalom, L. Embon, N. Shadmi, Y. Anahory, H. R. Naren, J. Sarkar, A. Uri, Y. Ronen, Y. Myasoedov, L. S. Levitov, E. Joselevich, A. K. Geim, and E. Zeldov, Nanoscale thermal imaging of dissipation in quantum systems, Nature **539**, 407 (2016).

[10] D. Halbertal, M. Ben Shalom, A. Uri, K. Bagani, A. Y. Meltzer, I. Marcus, Y. Myasoedov, J. Birkbeck, L. S. Levitov, A. K. Geim, and E. Zeldov, Imaging resonant dissipation from individual atomic defects in graphene, Science **358**, 1303 (2017).

[11] W. Thomson, On a mechanical theory of thermoelectric currents, Proc. R. Soc. **3**, 91 (1851).

[12] D. K. C. M. Donald, *Thermoelectricity: an Introduction to the Principles* (John Wiley and Sons, Inc., New York, 1962).

[13] B. J. van Wees, H. van Houten, C. W. J. Beenakker, J. G. Williamson, L. P. Kouwenhoven, D. van der Marel, and C. T. Foxon, Quantized Conductance of Point Contacts in a Two-dimensional Electron Gas, Phys. Rev. Lett. **60**, 848 (1988).

[14] D. A. Wharam, T. J. Thornton, R. Newbury, M. Pepper, H. Ahmed, J. E. F. Frost, D. G. Hasko, D. C. Peacock, D. A. Ritchie, and G. A. C. Jones, One-dimensional transport and the quantisation of the ballistic resistance, J. Phys. C: Solid State Phys. **21**, L209 (1988).

[15] M. Büttiker, Quantized transmission of a saddle-point constriction, Phys. Rev. B **41**, 7906 (1990).

[16] K. J. Thomas, J. T. Nicholls, M. Y. Simmons, M. Pepper, D. R. Mace, and D. A. Ritchie, Possible Spin Polarization in a One-dimensional Electron Gas, Phys. Rev. Lett. **77**, 135 (1996).

[17] S. M. Cronenwett, H. J. Lynch, D. Goldhaber-Gordon, L. P. Kouwenhoven, C. M. Marcus, K. Hirose, N. S. Wingreen, and V. Umansky, Low-temperature Fate of the 0.7 Structure in a Point Contact: A Kondo-like Correlated State in an Open System, Phys. Rev. Lett. **88**, 226805 (2002).

[18] T. Rejec and Y. Meir, Magnetic impurity formation in quantum point contacts, Nature **442**, 900 (2006).

[19] M. J. Iqbal, R. Levy, E. J. Koop, J. B. Dekker, J. P. de Jong, J. H. M. van der Velde, D. Reuter, A. D. Wieck, R. Aguado, Y. Meir, and C. H. van der Wal, Odd and even Kondo effects from emergent localization in quantum point contacts, Nature **501**, 79 (2013).

[20] F. Bauer, J. Heyder, E. Schubert, D. Borowsky, D. Taubert, B. Bruognolo, D. Schuh, W. Wegscheider, J. von Delft, and S. Ludwig, Microscopic origin of the 0.7-anomaly in quantum point contacts, Nature **501**, 73 (2013).

[21] B. Brun, F. Martins, S. Faniel, B. Hackens, G. Bachelier, A. Cavanna, C. Ulysse, A. Ouerghi, U. Gennser, D. Mailly, S. Huant, V. Bayot, M. Sanquer, and H. Sellier, Wigner and Kondo physics in quantum point contacts revealed by scanning gate microscopy, Nat. Commun. **5**, 4290 (2014).

[22] B. Brun, F. Martins, S. Faniel, B. Hackens, A. Cavanna, C. Ulysse, A. Ouerghi, U. Gennser, D. Mailly, P. Simon, S. Huant, V. Bayot, M. Sanquer, and H. Sellier, Electron Phase Shift at the Zero-Bias Anomaly of Quantum Point Contacts, Phys. Rev. Lett. **116**, 136801 (2016).

[23] A. P. Micolich, What lurks below the last plateExperimental studies of the $0.7 \times 2e^2/h$ conductance anomaly in one-dimensional systems, J. Phys.: Condens. Matter **23**, 443201 (2011).

[24] S. M. Cronenwett, PhD thesis, Harvard University, 2001.

[25] M. J. Iqbal, PhD thesis, Groningen University, 2014.

[26] P. Streda, Quantised thermopower of a channel in the ballistic regime, J. Phys.: Condens. Matter **1**, 1025 (1989).

[27] L. W. Molenkamp, H. van Houten, C. W. J. Beenakker, R. Eppenga, and C. T. Foxon, Quantum Oscillations in the Transverse Voltage of a Channel in the Nonlinear Transport Regime, Phys. Rev. Lett. **65**, 1052 (1990).

[28] L. W. Molenkamp, T. Gravier, H. van Houten, O. J. A. Buijk, M. A. A. Mabesoone, and C. T. Foxon, Peltier Coefficient and Thermal Conductance of a Quantum Point Contact, Phys. Rev. Lett. **68**, 3765 (1992).

[29] H. Mott and N. F. Jones, *The Theory of the Properties of Metals and Alloys* (Oxford University Press, Oxford, 1936).

[30] C. W. J. Beenakker and A. A. M. Staring, Theory of the thermopower of a quantum dot, Phys. Rev. B **46**, 9667 (1992).

[31] A. S. Dzurak, C. G. Smith, C. H. W. Barnes, M. Pepper, L. Martín-Moreno, C. T. Liang, D. A. Ritchie, and G. A. C. Jones, Thermoelectric signature of the excitation spectrum of a quantum dot, Phys. Rev. B **55**, R10197 (1997).

[32] D. Sanchez and R. Lopez, Nonlinear phenomena in quantum thermoelectrics and heat, C. R. Phys. **17**, 1060 (2016).

[33] D. Boese and R. Fazio, Thermoelectric effects in Kondo-correlated quantum dots, Europhys. Lett. **56**, 576 (2001).

[34] N. J. Appleyard, J. T. Nicholls, M. Pepper, W. R. Tribe, M. Y. Simmons, and D. A. Ritchie, Direction-resolved

transport and possible many-body effects in one-dimensional thermopower, Phys. Rev. B **62**, R16275 (2000).
[35] M. A. Topinka, B. J. LeRoy, R. M. Westervelt, S. E. J. Shaw, R. Fleischmann, E. J. Heller, K. D. Maranowski, and A. C. Gossard, Coherent branched flow in a two-dimensional electron gas, Nature **410**, 183 (2001).
[36] H. Sellier, B. Hackens, M. G. Pala, F. Martins, S. Baltazar, X. Wallart, L. Desplanque, V. Bayot, and S. Huant, On the imaging of electron transport in semiconductor quantum structures by scanning-gate microscopy: Successes and limitations, Semicond. Sci. Technol. **26**, 064008 (2011).
[37] A. Abbout, PhD thesis, University of Paris VI, 2011.
[38] M. P. Jura, M. A. Topinka, M. Grobis, L. N. Pfeiffer, K. W. West, and D. Goldhaber-Gordon, Electron interferometer formed with a scanning probe tip and quantum point contact, Phys. Rev. B **80**, 041303 (2009).
[39] A. A. Kozikov, C. Rössler, T. Ihn, K. Ensslin, C. Reichl, and W. Wegscheider, Interference of electrons in backscattering through a quantum point contact, New J. Phys. **15**, 013056 (2013).
[40] K. Hirose, Y. Meir, and N. S. Wingreen, Local Moment Formation in Quantum Point Contacts, Phys. Rev. Lett. **90**, 026804 (2003).
[41] T. Morimoto, Y. Iwase, N. Aoki, T. Sasaki, Y. Ochiai, A. Shailos, J. P. Bird, M. P. Lilly, J. L. Reno, and J. A. Simmons, Nonlocal resonant interaction between coupled quantum wires, Appl. Phys. Lett. **82**, 3952 (2003).
[42] B. Hackens, F. Martins, S. Faniel, C. A. Dutu, H. Sellier, S. Huant, M. Pala, L. Desplanque, X. Wallart, and V. Bayot, Imaging Coulomb islands in a quantum Hall interferometer, Nat. Commun. **1**, 39 (2010).
[43] See Supplemental Material at http://link.aps.org/supplemental/10.1103/PhysRevApplied.11.034069 for additional data and analysis, which also includes Refs. [69–74].
[44] A. M. Lunde and K. Flensberg, On the Mott formula for the thermopower of non-interacting electrons in quantum point contacts, J. Phys.: Condens. Matter **17**, 3879 (2005).
[45] P. J. Price, Hot electrons in a GaAs heterolayer at low temperature, J. Appl. Phys. **53**, 6863 (1982).
[46] A. Mittal, R. Wheeler, M. Keller, D. Prober, and R. Sacks, Electron-phonon scattering rates in GaAs/AlGaAs 2DEG samples below 0.5 K, Surf. Sci. **361**, 537 (1996).
[47] V. C. Karavolas and P. N. Butcher, Diffusion thermopower of a 2DEG, J. Phys.: Condens. Matter **3**, 2597 (1991).
[48] R. Fletcher, P. T. Coleridge, and Y. Feng, Oscillations in the diffusion thermopower of a two-dimensional electron gas, Phys. Rev. B **52**, 2823 (1995).
[49] M. Schmidt, G. Schneider, C. Heyn, A. Stemmann, and W. Hansen, Thermopower of a 2D Electron Gas in Suspended AlGaAs/GaAs Heterostructures, J. Electron. Mater. **41**, 1286 (2012).
[50] B. A. Braem, C. Gold, S. Hennel, M. Röösli, M. Berl, W. Dietsche, W. Wegscheider, K. Ensslin, and T. Ihn, Stable branched electron flow, New J. Phys. **20**, 073015 (2018).
[51] B. A. Braem, F. M. Pellegrino, A. Principi, M. Röösli, S. Hennel, J. V. Koski, M. Berl, W. Dietsche, W. Wegscheider, M. Polini, T. Ihn, and K. Ensslin, Scanning gate microscopy in a viscous electron fluid, Phys. Rev. B **98**, 241304(R) (2018).
[52] B. Brun, PhD thesis, University of Grenoble, 2014.
[53] A. Yacoby, M. Heiblum, D. Mahalu, and H. Shtrikman, Coherence and Phase Sensitive Measurements in a Quantum Dot, Phys. Rev. Lett. **74**, 4047 (1995).
[54] M. Zaffalon, A. Bid, M. Heiblum, D. Mahalu, and V. Umansky, Transmission Phase of a Singly Occupied Quantum Dot in the Kondo Regime, Phys. Rev. Lett. **100**, 226601 (2008).
[55] V. I. Puller, L. G. Mourokh, A. Shailos, and J. P. Bird, Detection of Local-moment Formation using the Resonant Interaction between Coupled Quantum Wires, Phys. Rev. Lett. **92**, 096802 (2004).
[56] H. Steinberg, O. M. Auslaender, A. Yacoby, J. Qian, G. A. Fiete, Y. Tserkovnyak, B. I. Halperin, K. W. Baldwin, L. N. Pfeiffer, and K. W. West, Localization transition in a ballistic quantum wire, Phys. Rev. B **73**, 113307 (2006).
[57] Y. Yoon, L. Mourokh, T. Morimoto, N. Aoki, Y. Ochiai, J. L. Reno, and J. P. Bird, Probing the Microscopic Structure of Bound States in Quantum Point Contacts, Phys. Rev. Lett. **99**, 136805 (2007).
[58] P. M. Wu, P. Li, H. Zhang, and A. M. Chang, Evidence for the formation of quasibound states in an asymmetrical quantum point contact, Phys. Rev. B **85**, 085305 (2012).
[59] S.-C. Ho, H.-J. Chang, C.-H. Chang, S.-T. Lo, G. Creeth, S. Kumar, I. Farrer, D. Ritchie, J. Griffiths, G. Jones, M. Pepper, and T.-M. Chen, Imaging the Zigzag Wigner Crystal in Confinement-Tunable Quantum Wires, Phys. Rev. Lett. **121**, 106801 (2018).
[60] S. A. Söffing, M. Bortz, I. Schneider, A. Struck, M. Fleischhauer, and S. Eggert, Wigner crystal versus Friedel oscillations in the one-dimensional Hubbard model, Phys. Rev. B **79**, 195114 (2009).
[61] O. P. Sushkov, Conductance anomalies in a one-dimensional quantum contact, Phys. Rev. B **64**, 155319 (2001).
[62] O. P. Sushkov, Restricted and unrestricted Hartree-Fock calculations of conductance for a quantum point contact, Phys. Rev. B **67**, 195318 (2003).
[63] L. Shulenburger, M. Casula, G. Senatore, and R. M. Martin, Correlation effects in quasi-one-dimensional quantum wires, Phys. Rev. B **78**, 165303 (2008).
[64] A. D. Güçlü, C. J. Umrigar, H. Jiang, and H. U. Baranger, Localization in an inhomogeneous quantum wire, Phys. Rev. B **80**, 201302 (2009).
[65] K.-F. Berggren and I. I. Yakimenko, Nature of electron states and symmetry breaking in quantum point contacts according to the local spin density approximation, J. Phys.: Condens. Matter **20**, 164203 (2008).
[66] I. I. Yakimenko, V. S. Tsykunov, and K.-F. Berggren, Bound states, electron localization and spin correlations in low-dimensional GaAs/AlGaAs quantum constrictions, J. Phys.: Condens. Matter **25**, 072201 (2013).
[67] Y. Yoon, M.-G. Kang, T. Morimoto, L. Mourokh, N. Aoki, J. L. Reno, J. P. Bird, and Y. Ochiai, Detector backaction on the self-consistent bound state in quantum point contacts, Phys. Rev. B **79**, 121304 (2009).
[68] Y. Ren, W. W. Yu, S. M. Frolov, J. A. Folk, and W. Wegscheider, Zero-bias anomaly of quantum point

contacts in the low-conductance limit, Phys. Rev. B **82**, 045313 (2010).

[69] E. Wigner, On the interaction of electrons in metals, Phys. Rev. **46**, 1002 (1934).

[70] B. Tanatar and D. M. Ceperley, Ground state of the two-dimensional electron gas, Phys. Rev. B **39**, 5005 (1989).

[71] M. Kawamura, K. Ono, P. Stano, K. Kono, and T. Aono, Electronic Magnetization of a Quantum Point Contact Measured by Nuclear Magnetic Resonance, Phys. Rev. Lett. **115**, 036601 (2015).

[72] D. H. Schimmel, B. Bruognolo, and J. von Delft, Spin Fluctuations in the 0.7 Anomaly in Quantum Point Contacts, Phys. Rev. Lett. **119**, 196401 (2017).

[73] A. Freyn, I. Kleftogiannis, and J.-L. Pichard, Scanning Gate Microscopy of a Nanostructure Where Electrons Interact, Phys. Rev. Lett. **100**, 226802 (2008).

[74] These expressions are valid in the linear-response regime. Although the experimental conditions do not satisfy the condition $\Delta T \ll T$, this linear model can partly explain the observations, which justifies *a posteriori* this approximation